



Cite this: DOI: 10.1039/c9nj06396j

Tuning of the redox potential and catalytic activity of a new Cu(II) complex by *o*-iminobenzosemiquinone as an electron-reservoir ligand†

 Mina Nasibipour,^a Elham Safaei,^{ib}*^a Grzegorz Wrzeszcz^{ib}^b and Andrzej Wojtczak^{ib}^b

The synthesis and characterization of a new Cu(II) complex, L₂^{NIS}Cu^{II} (L^{NIS} = *o*-iminobenzosemiquinone), are reported. X-ray crystallography studies showed that two *o*-iminobenzosemiquinone radicals form a distorted square-planar geometry around the Cu(II) center of L₂^{NIS}Cu^{II}. Magnetic measurements revealed the paramagnetic character of the complex caused by the presence of three unpaired electrons located on the *o*-iminobenzosemiquinonate ligands and the Cu^{II} center. Magnetochemical experiments, and EPR and DFT studies prove that the ground state of the complex is a doublet, which is consistent with the ferromagnetic coupling between Cu(II) and *o*-iminobenzosemiquinone centers and stronger antiferromagnetic coupling between the iminobenzosemiquinone moieties. The ligand-centered redox reactions of the complex were studied by cyclic voltammetry. Aerobic oxidation of alcohols to aldehydes with TEMPO was studied in the presence of L₂^{NIS}Cu^{II}. Furthermore, L₂^{NIS}Cu^{II} was found to be an efficient catalyst in homo-coupling of terminal alkynes.

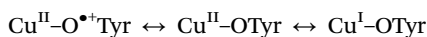
 Received 26th December 2019,
Accepted 7th February 2020

DOI: 10.1039/c9nj06396j

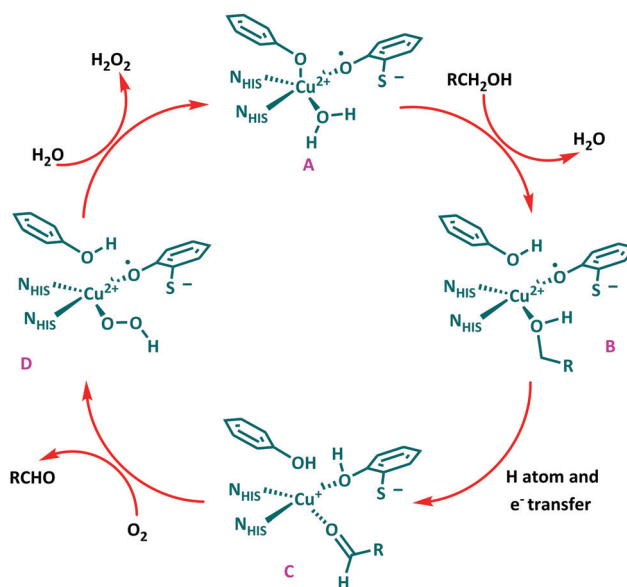
rsc.li/njc

Introduction

One of the most important areas of research in bio-coordination chemistry is the study of the interaction of pro-radical ligands with metal ions and investigation of their effects on the reactivity of the metal center as well as the whole complex.¹ The main concept is that the cooperation between metal and ligand in such complexes can modify the overall properties of the system and improve their applicability as models of different enzymes such as galactose oxidase (GOase).² GOase is an enzyme with two tyrosinate moieties, two histidine units, and H₂O molecules surrounding the Cu(II) ion in a square-pyramidal geometry in its active site (Scheme 1). The enzyme activity is related to three stable oxidation states of A, Cu(II)-tyrosyl; B, Cu(II) tyrosine; and C, Cu(I) tyrosine.³



GOase performs the oxidation of primary alcohols to the corresponding aldehydes through a Cu(II) phenoxyl-radical with concomitant generation of H₂O₂ and eventual reduction of O₂


 Scheme 1 The GOase-active site and different redox states.^{3a}

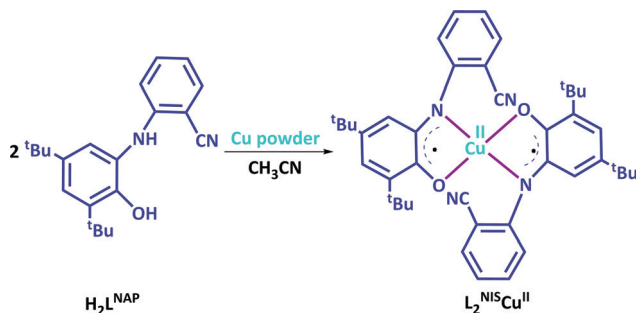
to water.⁴ Due to the importance of insight into the structure and electronic properties of the active site of the enzyme, several models of galactose oxidase enzyme have been provided in the last few years.⁵

The presence of metals with variable oxidation states and proper ligands with variable oxidation states which permit

^a Department of Chemistry, College of Sciences, Shiraz University, Shiraz, 71454, Iran. E-mail: e.safaei@shirazu.ac.ir

^b Faculty of Chemistry, Nicolaus Copernicus University in Torun, 87-100 Torun, Poland

† Electronic supplementary information (ESI) available. CCDC 1870228. For ESI and crystallographic data in CIF or other electronic format see DOI: 10.1039/c9nj06396j



Scheme 2 The structures of $\text{H}_2\text{L}^{\text{NAP}}$ and its $\text{L}_2^{\text{NIS}}\text{Cu}^{\text{II}}$ complex.

tuning the oxidation states of the metal center (non-innocent ligands) in coordination complexes are among the main requirements to achieve higher catalytic activity. Accordingly, the design and synthesis of enzyme model complexes containing non-innocent ligands have attracted significant attention.⁶ In this regard, several *o*-aminophenol ligands and their corresponding metal complexes have been synthesized. The catalytic activities of these ligand copper complexes in aerobic oxidation of alcohols have also been investigated.⁷

In recent decades, alkyne building blocks have received more attention in industrial, agricultural and molecular devices. Conjugated 1,3-diyne obtained from acetylene coupling are one of the most important intermediates or materials.⁸

One of the oldest reactions for the preparation of bis acetylenes is Glaser coupling, a homo coupling of terminal alkenes using Cu(I) in a polar solvent and the presence of oxygen to reoxidize the copper center in a catalytic cycle. In Hey coupling, a versatile reaction in a wide range of solvents was provided using a Cu(I)-TMEDA system. In the related Ellington reaction, a Cu(II) pyridine system was applied for coupling of terminal alkynes.^{9–14}

Herein, we report the synthesis and characterization of a new Cu(II) complex of redox-active *o*-aminophenolate $\text{H}_2\text{L}^{\text{NAP}}$, in which NAP stands for the aminophenol form of the ligand (Scheme 2). Moreover, the catalytic activity of $\text{L}_2^{\text{NIS}}\text{Cu}^{\text{II}}$ (in which L^{NIS} is *o*-iminobenzosemiquinone, a one electron oxidized form of the coordinated L^{NAP}) in the aerobic oxidation of a broad range of alcohols to the corresponding aldehydes under mild conditions has been studied. Also, the complex was used as a catalyst in the homo-coupling process of terminal alkynes.

Results and discussion

Synthesis and characterization of $\text{H}_2\text{L}^{\text{NAP}}$

The $\text{H}_2\text{L}^{\text{NAP}}$ ligand was synthesized *via* the condensation reaction of 2-aminobenzonitrile and 3,5-di-*tert*-butylcatechol as explained in the literature.¹⁵ The ligand was characterized by spectroscopic and elemental analysis. The ligand $\text{H}_2\text{L}^{\text{NAP}}$ exhibits characteristic IR bands at $\nu = 3421\text{ cm}^{-1}$ and $\nu = 3354\text{ cm}^{-1}$ that belong to $\nu_{\text{O-H}}$ and $\nu_{\text{N-H}}$ vibrational stretches, respectively. The presence of a -CN group is confirmed by the stretching band at $\nu = 2222\text{ cm}^{-1}$. The *tert*-butyl group bands appear at $\nu = 2865\text{ cm}^{-1}$, $\nu = 2904$ and $\nu = 2950$ and the phenolic $\nu(\text{C-O})$ stretching band appears at $\nu = 1272\text{ cm}^{-1}$.

The bands at $\nu = 760\text{ cm}^{-1}$ and $\nu = 1600\text{ cm}^{-1}$ show $=\text{C-H}$ bending and $\text{C}=\text{C}$, respectively.

Synthesis and characterization of $\text{L}_2^{\text{NIS}}\text{Cu}^{\text{II}}$

Treatment of $\text{H}_2\text{L}^{\text{NAP}}$ with Cu powder in an equimolar ratio under aerobic conditions in acetonitrile at room temperature afforded needle crystals of $\text{L}_2^{\text{NIS}}\text{Cu}^{\text{II}}$ (eqn (1)):



Elemental analysis confirms the 1 : 2 molar ratio of metal to ligand in the complex. All the vibrations of the ligand are present in the IR spectrum, confirming the presence of the ligand in the complex. Disappearance of the strong $\nu_{\text{O-H}}$ stretching band in the IR spectrum of the complex shows the deprotonation of the ligand and coordination of the resultant phenolate to the Cu(II) center.

In the IR spectrum of the complex, the phenolic $\nu(\text{C-O})$ stretching band appears at $\nu = 1254\text{ cm}^{-1}$. The bands appearing at $\nu = 2958$, 2940 , and 2872 cm^{-1} can be attributed to the presence of 2,4-di *tert*-butylphenolate group in the ligand structure. In the spectra of the complex a strong band appears at $\nu = 2226$ indicating the presence of the -CN group and no ligation from its N atom to Cu. Similar to the IR spectrum of the ligand, the $\nu(\text{C-C})$, $\nu(=\text{C-H})$ bending and $\nu(\text{C}=\text{C})$ stretching bands appear at $\nu = 1480\text{ cm}^{-1}$, $\nu = 766\text{ cm}^{-1}$ and $\nu = 1601\text{ cm}^{-1}$, respectively. The $\nu = 3354\text{ cm}^{-1}$ of the N-H group in the ligand has disappeared in the complex structure which is attributed to the conversion of the *o*-aminophenol ligand coordinated with Cu(II) to other tautomeric deprotonated forms. In the IR spectrum of the complex, we observe contributions from the C-O stretching of semiquinone at 1478 cm^{-1} . The band seen at 3438 cm^{-1} is related to O-H of MeOH or H_2O , despite the analysis being done in very dry conditions.

Crystal structure of $\text{L}_2^{\text{NIS}}\text{Cu}^{\text{II}}$

Green crystals were obtained from a methanol-dichloromethane (1 : 1) mixture. Crystallographic data are shown in Table 1. Selected bond distances and angles are listed in Table 2. The solid state structure of $\text{L}_2^{\text{NIS}}\text{Cu}^{\text{II}}$ is shown in Fig. 1. The molecule of the $\text{L}_2^{\text{NIS}}\text{Cu}^{\text{II}}$ complex has a C_i symmetry with the Cu ion located on the center of symmetry. Therefore, the asymmetric unit consists of half of the molecule (half of the Cu ion and one ligand). The C18 of the *tert*-Bu group reveals the rotational disorder, with two discrete populations of 57/43% occupancy. The coordination sphere CuN_2O_2 has a square-planar geometry with bi-dentate L^{NIS} iminosemiquinone coordinated *via* O and N atoms, while the nitrile substituent does not form any interaction with Cu(II) (Fig. 1).

Two chelate 5-membered rings formed by L^{NAP} are flat. In the coordination sphere, the Cu1-O1 and Cu1-N1 bond lengths are almost identical, being $1.9210(19)$ and $1.928(2)\text{ \AA}$, respectively. The N1-Cu1-O1 and N1-Cu1-O1[-*x*, -*y*, -*z*] angles are $83.18(8)$ and $96.82(8)^\circ$, respectively, with the difference reflecting the proximity of both donor atoms within one ligand molecule. The valence geometry of the aminophenol ligand is typical for such systems (Table 2). However, the C1-O1 and C6-N1 bonds of

Table 1 Crystallographic data for $L_2^{NIS}Cu^{II}$

Empirical formula	$C_{42}H_{48}CuN_4O_2$
Formula weight	704.38
Crystal system	Triclinic
Space group	$P\bar{1}$
Unit cell dimensions	$a = 8.5030(5) \text{ \AA}$ $b = 10.8824(8) \text{ \AA}$ $c = 11.7661(10) \text{ \AA}$ $\alpha = 114.768(8)^\circ$ $\beta = 90.404(6)^\circ$ $\gamma = 92.966(5)^\circ$
Volume	$986.78(14) \text{ \AA}^3$
Z	1
Temperature	293(2) K
Density (calculated)	1.185 Mg m^{-3}
Crystal size	$0.518 \times 0.298 \times 0.130 \text{ mm}^3$
Absorption coefficient	0.591 mm^{-1}
Reflections collected	6811
Independent reflections	4344 [$R(\text{int}) = 0.0512$]
Goodness-of-fit on F^2	1.003
Final R indices [$I > 2\sigma(I)$]	$R_1 = 0.0554$, $wR_2 = 0.1439$
R indices (all data)	$R_1 = 0.0799$, $wR_2 = 0.1741$

Table 2 Selected bond lengths [Å] and angles [°] for $L_2^{NIS}Cu^{II}$

Cu1–O1	1.9210(19)
Cu1–N1	1.928(2)
O1–C1	1.298(3)
C6–N1	1.340(3)
C1–C2	1.424(4)
C1–C6	1.448(4)
C2–C3	1.371(4)
C3–C4	1.428(4)
C4–C5	1.361(4)
C5–C6	1.416(4)
O1–Cu1–N1#1	96.82(8)
O1–Cu1–N1	83.18(8)
O1#1–Cu1–N1	96.82(8)
N2–C13–C12	178.4(4)

Symmetry transformations used to generate equivalent atoms: #1 – x , $-y$, $-z$.

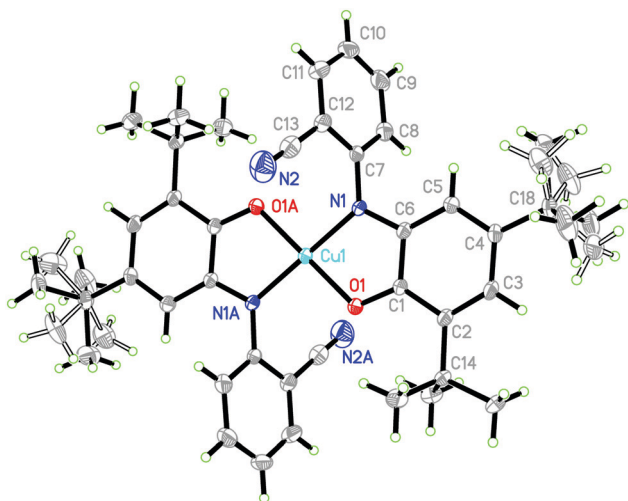


Fig. 1 Molecular structure of $L_2^{NIS}Cu^{II}$. Thermal ellipsoids are set at 50% probability.

1.298(3) and 1.340(3) Å, respectively, are shorter than expected for the single bonds. Also, the consecutive bonds in the C2–C1–C6–C5

fragment (1.424(4), 1.448(4) and 1.416(4) Å, respectively), as well as significantly shorter C2–C3 and C4–C5 (1.371(4) and 1.361(4) Å, respectively) indicate that the ligand exists in the *o*-iminobenzosemiquinoate radical mono anion L^{NIS} form. That is consistent with the results of the metrical oxidation state method¹⁶ used for calculation of the experimental MOS of the aminophenolate ligand, which is $-0.89(4)$.

Such a form was also detected, among others, for Cu complexes with L^{BIS} ligands,^{7b,17} or transition metal complexes with *o*-aminophenols.^{16,18,19} The geometry of the nitrile substituent in L^{NAP} is typical, and the N2–C13–C12 angle is 178.4(4)°. Conformation of the ligand can be described with two torsion angles C1–C6–N1–C7 and C6–N1–C7–C8 in the bridging amine fragment, with the values being $-177.4(2)$ and $64.61(2)^\circ$, respectively. In the observed conformation, the dihedral angle between two phenyl moieties is 67.8(2)°. The dihedral angles between the amino-phenyl C1–C6 and C7–C12 phenyl rings and the N_2O_2 coordination plane are 0.4(1) and 67.5(2)°, respectively. Two intramolecular C16–H16C...O1 and C17–H17B...O1 interactions are found with the C...O distances being 2.972(4) and 3.123(4) Å, respectively. All data for bond angles and lengths are shown in Tables S1 and S2 (ESI[†]). The monohydrate structure $L_2^{NIS}Cu^{II} \cdot H_2O$ in the monoclinic $P2_1/c$ space group was determined and included in the PhD thesis <http://gyan.iitg.ernet.in/handle/123456789/557>.^{19a} In that report, the ligand was found in the same one-electron oxidized form. However, it is not deposited in the CSD. Therefore, the structure reported here is the only structure available to the scientific community.

Magnetic measurements

Magnetic properties of the $L_2^{NIS}Cu^{II}$ complex were measured in the temperature range of 1.9–300 K with 10 000 Oe magnetic field. In a temperature range of 10–150 K, the product of magnetic susceptibility and temperature ($\chi \cdot T$) for the $L_2^{NIS}Cu^{II}$ complex remains nearly constant at $0.34 \text{ emu K mol}^{-1}$ (1.64 BM) (Fig. 2), a value that corresponds to an isolated $S = 1/2$ ground spin state. Below 10 K, the $\chi \cdot T$ slowly decreases reaching $0.30 \text{ emu K mol}^{-1}$

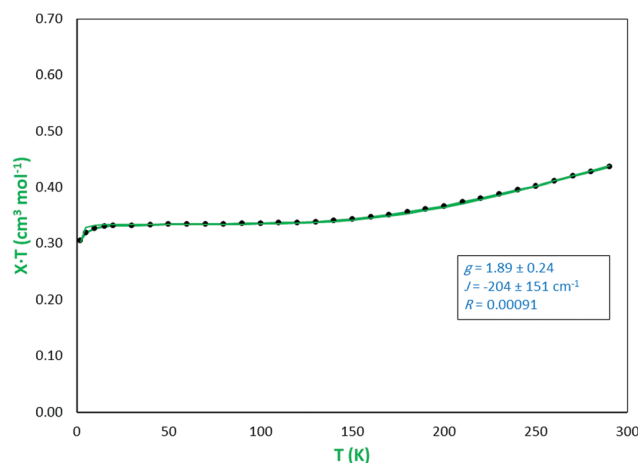
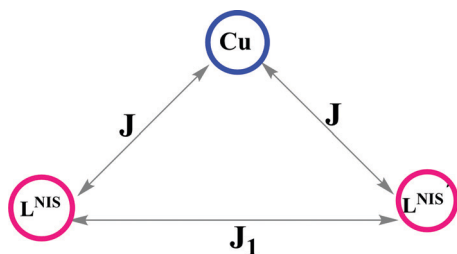


Fig. 2 Magnetic susceptibility plot of $L_2^{NIS}Cu^{II}$ with best fitted parameters: $g = 1.893$, $J = 363$, and $J_1 = -499 \text{ cm}^{-1}$. The data are given by the dots and the line is a theoretical fit to the model described in the text.

(1.55 BM), probably due to antiferromagnetic intermolecular interactions. With increasing temperature (150 to 300 K, Fig. 2), the $\chi \cdot T$ reaches a value of 0.436 emu K mol⁻¹ (1.87 BM), which is slightly larger than the value of 0.37 emu K mol⁻¹ (1.73 BM) expected for one uncoupled spin-only Cu(II) ion ($S = 1/2$).^{5,6d} Hence, when the temperature increases, another spin state is populated and it leads to an increase in the magnetic moment. These data suggest the overall antiferromagnetic coupling between the spins of two iminobenzosemiquinonate radicals and the Cu(II) center. This result is consistent with the X-ray results that Cu(II) is surrounded by two iminosemiquinone radicals (L^{NIS} and $L^{\text{NIS}'}$), each having a spin of $S = 1/2$. Therefore, it is a three spin complex with three possible spin compositions of $\uparrow\uparrow\uparrow$, $\uparrow\downarrow\uparrow$, $\uparrow\uparrow\downarrow$ ²⁰ in which the $S_{\text{tot}} = S_{\text{Cu}} + S_{L^{\text{NIS}}} + S_{L^{\text{NIS}'}}$, $S_{L^{\text{NIS}'}}^* = S_{L^{\text{NIS}}} + S_{L^{\text{NIS}'}}$, and $(S_{\text{tot}}, S^*) = (3/2, 1), (1/2, 1), (1/2, 0)$ (Scheme 3).

According to Scheme 3, the experimental magnetic data have been fitted using the Heisenberg Hamiltonian: $\hat{H} = -2J(\hat{S}_1 \cdot \hat{S}_2 + \hat{S}_1 \cdot \hat{S}_3) - 2J_1 \hat{S}_2 \cdot \hat{S}_3$, where \hat{S}_1 corresponds to spin of Cu, while \hat{S}_2 and \hat{S}_3 correspond to two spins on the radicals. The magnetic susceptibility data throughout the entire temperature range were fitted with this model (Fig. 2) using the PHI program.²¹ Several constraints were placed on the fit to avoid over-parameterization. First, only a single g value for both L^{NIS} radicals and the Cu(II) center was included in the model and the fixed molecular field parameter was applied ($zJ' = -0.1 \text{ cm}^{-1}$). The J value is the coupling constant of Cu and L^{NIS} and J_1 is the coupling constant of two L^{NIS} and $L^{\text{NIS}'}$ ligands. Due to the opposing ferromagnetic and antiferromagnetic effects, the model fit to the experimental data is good for a relatively broad range of tested J and J_1 parameters. The best fitted parameters are as follows: $g = 1.893$, $J = 363$, and $J_1 = -499 \text{ cm}^{-1}$ (Fig. 2). Fitting clearly indicates the presence of the large antiferromagnetic coupling between the L^{NIS} ligand radicals and the ferromagnetic coupling between the Cu(II) center and the L^{NIS} ligand radicals. Similar results have been published for copper complexes with analogous ligands.¹⁸ The set of models is consistent with the results of theoretical calculations presented below. An acceptable fit to the experimental data was also obtained for opposite models, which were insensitive to the J_1 parameter and therefore only J was used in the fit. However, the best value of $J = -204 \text{ cm}^{-1}$ was obtained, which might indicate the antiferromagnetic coupling between the copper center and ligand radicals. These models were rejected as being contradictory to the DFT and EPR results.



Scheme 3 Representation of variation in redox state in the $L_2^{\text{NIS}}\text{Cu}^{\text{II}}$ complex.

Electrochemistry

Electrochemical properties of the $L_2^{\text{NIS}}\text{Cu}^{\text{II}}$ complex were studied in CH_2Cl_2 by cyclic voltammetry (CV) at 233 K. In the studied potential range, four quasi-reversible one-electron redox processes were observed for the complex (Fig. 3 and Table 3). Based on the reported results for similar complexes, the negative potential peaks can be assigned to the ligand based iminosemiquinone/amidophenoxide redox couples.²² In addition, ligand-centered voltammograms are observed in the positive potential range showing the iminobenzosemiquinone/iminoquinone redox couple (Scheme 4).^{18,22} Therefore, we can see four peak potentials for the two above-mentioned ligand reduction and oxidation processes.

Electronic spectroscopy

The electronic spectrum of $L_2^{\text{NIS}}\text{Cu}^{\text{II}}$ in CH_2Cl_2 exhibits a series of bands in the ultraviolet and visible regions (Fig. 4). The absorption bands in 302 nm and 350 nm are attributed to the $\pi \rightarrow \pi^*$ intra-ligand charge transitions (ILCT). The electronic absorption spectrum at 450 nm is related to the ligand to metal charge transfer (LMCT) from phenolate orbitals to the d orbitals of Cu(II). The broad band at lower energy (810 nm) refers to the MLCT charge transfer.^{5,6,18}

EPR analysis

A frozen CH_2Cl_2 solution of the neutral $L_2^{\text{NIS}}\text{Cu}^{\text{II}}$ is EPR active (Fig. 5 and Table 4), due to the paramagnetic electronic ground state ($S = 1/2$) caused by antiferromagnetic coupling between two iminobenzosemiquinone ligands and Cu(II) unpaired electrons. The observed four-line signals display hyperfine splitting due to the $I = 3/2$ Cu center which is characteristic of monomeric Cu(II) complexes. Simulation of the experimental data results in the following parameters: $g_x = 2.0365$, $g_y = 2.0760$, $g_z = 2.1960$, (A_x, A_y, A_z) ($\times 10^4; \text{cm}^{-1}$) (5.70, 18.0, 191).

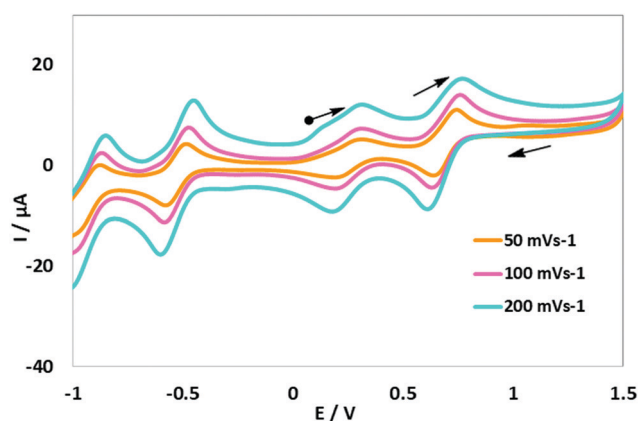
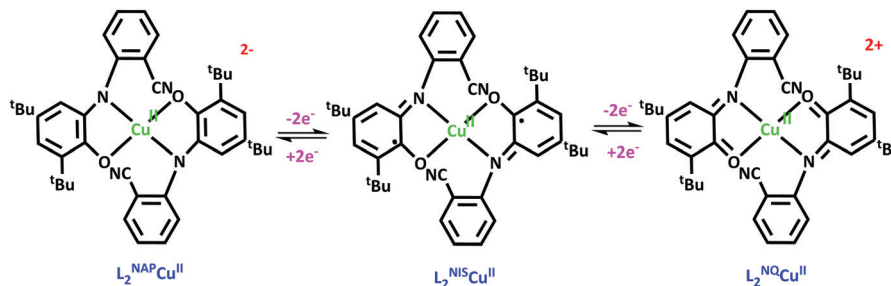


Fig. 3 Cyclic voltammograms of $L_2^{\text{NIS}}\text{Cu}^{\text{II}}$. Conditions: 1 mM complex, 0.1 M NBu_4ClO_4 , scan rates 50, 100, and 150 mV s^{-1} , CH_2Cl_2 , and 298 K.

Table 3 Redox potentials of $L_2^{\text{NIS}}\text{Cu}^{\text{II}}$ versus Fc^+/Fc

Compound	$E_{1/2}^1/\text{V}$	$E_{1/2}^2/\text{V}$	$E_{1/2}^3/\text{V}$	$E_{1/2}^4/\text{V}$
$L_2^{\text{NIS}}\text{Cu}^{\text{II}}$	-0.83	-0.44	0.33	0.77



Scheme 4 Schematic representation of $L_2^{NIS}Cu^{II}$ complex oxidation state variation.

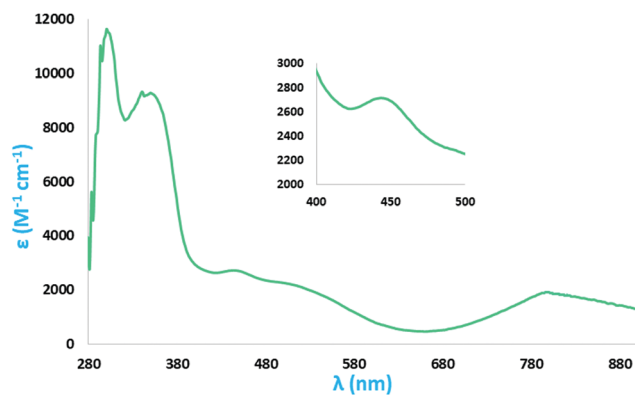


Fig. 4 Electronic spectrum of 2 mM CH_2Cl_2 solutions of $L_2^{NIS}Cu^{II}$. Inset shows the zoom-in 400–500 nm region.

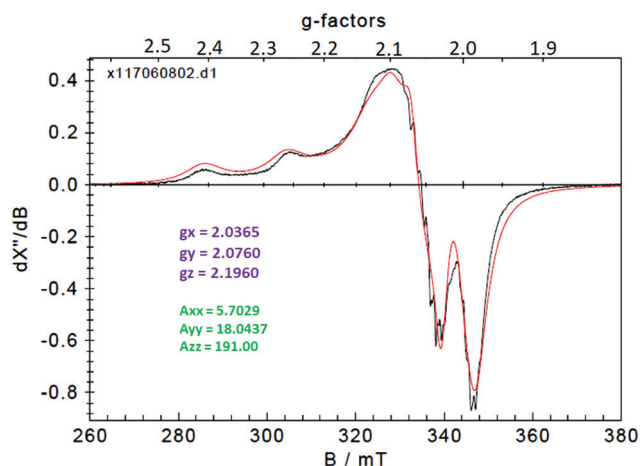


Fig. 5 EPR spectrum of $L_2^{NIS}Cu^{II}$ at frequency = 9.63649 GHz; power = 2 mW; modulation frequency = 100 kHz; amplitude = 3.0 G; $T = 30$ K; 1 mM.

Table 4 EPR data for $L_2^{NIS}Cu^{II}$. The A_i values [cm^{-1}] multiplied by 10^4

g_x	g_y	g_z	$A_x(Cu)$	$A_y(Cu)$	$A_z(Cu)$
2.0365	2.0760	2.1960	5.70	18.0	191

These parameters are a clear sign of the asymmetric coordination of ligands around the Cu^{II} center in a distorted square-planar geometry. The presence of an unpaired electron at the $d_{x^2-y^2}$ orbital of the $Cu(II)$ ion was deduced from the trends of $g_z > g_x, g_y > 2.0023$ and $A_z \gg A_x, A_y$.^{5,6}

Theoretical analysis

The orbital shapes and energies are given in Fig. 6. Orbital number 189 corresponds to the LUMO. The highest occupied orbitals in this complex are presented by single occupied molecular orbitals (SOMO). There are three paramagnetic centers in the $L_2^{NIS}Cu^{II}$ complex; each of them comprises one unpaired electron: one electron is located at the copper atom and two others at radical-anion iminobenzosemiquinone ligands.²³ These electrons occupy SOMOs 188 α , 187 α and 186 α . The orbital number 185 is the highest doubly occupied orbital (HOMO), which is obtained by a combination of corresponding α and β . Orbitals 188 α , 187 α and 186 α are so-called “magnetic” orbitals, determining the nature of exchange interactions (Fig. 6). Exchange coupling of unpaired electrons in the paramagnetic centers was estimated using the “broken symmetry” (BS) approach.²⁴

We have calculated the states with different orientation spins of unpaired electrons – $\alpha\alpha\alpha$, $\beta\alpha\alpha$ and $\alpha\beta\alpha$, presented in Fig. 7 (where α is spin up, and β is spin down). Two types of exchange interactions are possible in the complex containing three paramagnetic centers: (1) between the copper atom and semiquinone ligand (J) and (2) between the two semiquinones (J_1) (Scheme 5).

The formula applied for the calculation of exchange interactions in such systems with the use of the generalized spin-projection approach developed by Yamaguchi²⁵ is presented below: (where E is the value of total energy of the corresponding state, and S^2 is the value of the spin-squared operator).

$$J = -(E_{\alpha\alpha\alpha} - E_{\alpha\beta\alpha}) / (\langle S^2 \rangle_{\alpha\alpha\alpha} - \langle S^2 \rangle_{\alpha\beta\alpha})$$

$$J_1 = -(E_{\alpha\alpha\alpha} - 2E_{\alpha\alpha\beta} + E_{\alpha\beta\alpha}) / (\langle S^2 \rangle_{\alpha\alpha\alpha} - 2\langle S^2 \rangle_{\alpha\alpha\beta} + \langle S^2 \rangle_{\alpha\beta\alpha})$$

The results of estimation of exchange spin coupling constants with the use of the 6-311++G(d,p) basis set and two functionals (B3LYP and TPSSh) are collected in Table 5. The calculations were performed on the experimental geometry (SP-single point), optimized for the complex (OPT). The obtained results point to the presence of ferromagnetic coupling between each iminobenzosemiquinone radical and the copper center, and stronger anti-ferromagnetic exchange coupling between the unpaired electrons of two iminobenzosemiquinone radicals (Table 5).

Investigation of the catalytic properties of the $L_2^{NIS}Cu^{II}$ complex

A. Alcohol oxidation. Aerobic oxidation of alcohols has been of interest to chemists.^{6i,26} In our research, the $L_2^{NIS}Cu^{II}$

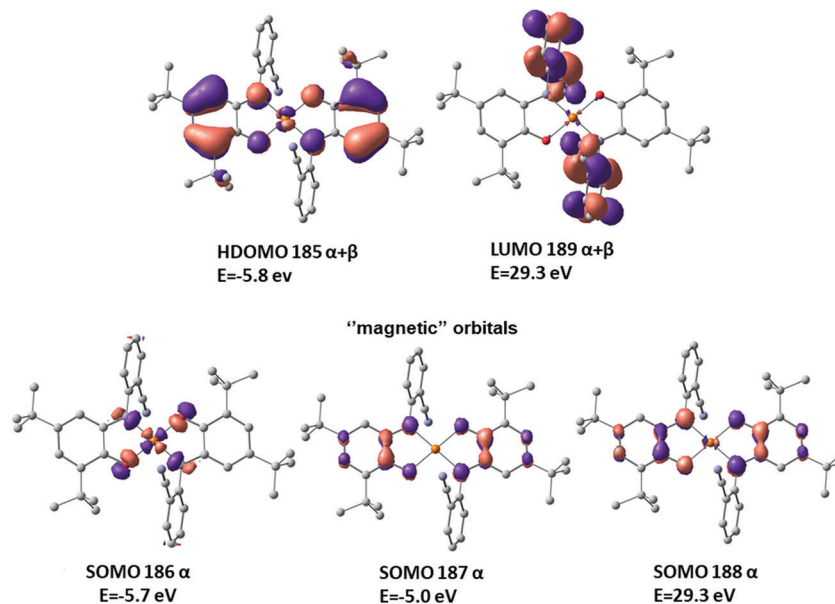


Fig. 6 The HOMO, LUMO and "magnetic" (SOMO) orbital shapes and energies.

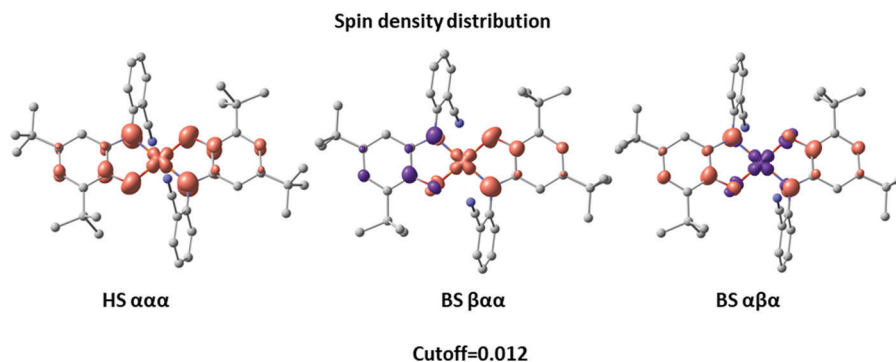
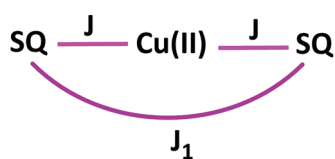


Fig. 7 Spin density distribution, cutoff = 0.012.



Scheme 5 Schematic representation of two types of L^{NIS}/L^{NIS} and Cu/L^{NIS} exchange interactions.

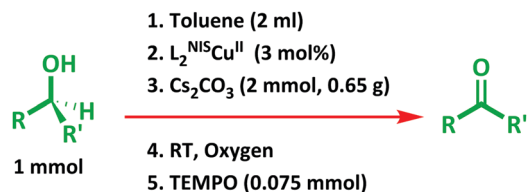
Table 5 Exchange spin coupling constants [cm^{-1}]

	SP		OPT	
	J	J_1	J	J_1
B3LYP	357	-447	331	-379
TPSSH	359	-575	332	-515

catalytic activity for oxidation of alcohols to the corresponding aldehydes was investigated. Firstly, the $L_2^{NIS}Cu^{II}$ mediated oxidation of benzyl alcohol as a model compound was performed and the reaction conditions of solvent, base, and catalyst

amount were optimized (Scheme 6). In the first step, the effect of bases such as Cs_2CO_3 , KOH and Na_2CO_3 for oxidation of benzyl alcohol was checked. In the presence of Cs_2CO_3 , the highest conversion of alcohol was observed. Optimization of the amount of Cs_2CO_3 showed that the best result was achieved with 2 equivalents of Cs_2CO_3 .

For investigating the solvent effect in this reaction, organic solvents such as CH_3CN , CH_2Cl_2 and toluene were applied and our result clearly confirmed that the most favorable solvent for this transformation is toluene (Table 6, entries 1–5). The amount of catalyst was also optimized and the highest conversion percentage was observed when 3 mol% of complex was used (Table 6, entries 10–12). In the next stage, the impact of different amounts of TEMPO (5×10^{-3} mmol, 0.05 mmol, 0.075 mmol and 0.1 mmol) was studied for the optimized condition (2 equivalents Cs_2CO_3 , toluene, and 3 equivalents catalyst). The best result was achieved when the amount of TEMPO was 0.075 mmol (Table 7, entry 5). The comparison of the results shows that changing the amount of TEMPO was much more important than the complex.



Scheme 6 Optimized conditions for catalytic activity of $L_2^{NIS}Cu^{II}$ in aerobic oxidation of alcohol.

Table 6 The effect of various bases and solvents for the aerobic oxidation of benzyl alcohol by $L_2^{NIS}Cu^{II}$

Entry	Base	Solvent	Catalyst (mol%)	Time (h)	Conversion (%)
1	2 eq. CS_2CO_3	Toluene	2	8	26
2	2 eq. KOH	Toluene	2	8	14
3	2 eq. K_2CO_3	Toluene	2	8	12
4	2 eq. Na_2CO_3	Toluene	2	8	12
5	3 eq. CS_2CO_3	Toluene	2	8	28
6	2 eq. CS_2CO_3	Acetonitrile	2	8	16
7	2 eq. KOH	Acetonitrile	2	8	16
8	2 eq. K_2CO_3	Acetonitrile	2	8	12
9	2 eq. Na_2CO_3	Acetonitrile	2	8	10
10	2 eq. CS_2CO_3	Dichloromethane	2	8	13
11	2 eq. CS_2CO_3	Toluene	3	8	29
12	2 eq. CS_2CO_3	Toluene	5	8	30

It is worth mentioning that performing the mentioned optimized reaction in the base-free condition led to a dramatic decrease in reaction conversion.

In blank tests, replacement of the copper complex with $Cu(II)$ acetate and the consequent decline in the aldehyde yield proves the important role of the ligand in the alcohol transformation. Increase of the aldehyde yield by addition of free ligand to $Cu(II)$ acetate proves this claim. Comparison of two mentioned blank test results (Table 8, entries 1 and 2) with the same complex of $L_2^{NIS}Cu^{II}$ as the catalyst (Table 9, entry 1), demonstrates the contribution of both the copper center and ligand due to the coordination process playing an important role in the oxidation of alcohols. A blank test using only TEMPO as the catalyst was performed. The contribution of TEMPO in alcohol oxidation was only 20% (Table 8, entry 3). This means that TEMPO plays a co-catalyst role in this reaction. In addition, oxidation of benzyl alcohol using TEMPO and $Cu(II)$ acetate as a catalyst provides only 33% aldehyde and after a long time the reactant has not converted. This result also shows the role of the complex in the mentioned oxidation reaction (Table 8, entry 5).

After optimizing the reaction conditions (3 mol% $L_2^{NIS}Cu^{II}$, 2 mmol CS_2CO_3 and 0.075 mmol TEMPO), we used other

Table 8 The result of blank tests for oxidation of benzyl alcohol with the catalyst system

Entry	Catalytic system	Time (h)	Conversion (%)
1	H_2L^{NAP} 3 mol%/ CS_2CO_3	8	28
2	$Cu(OAc)_2$ 3 mol%/ CS_2CO_3	8	24
3	TEMPO 0.075 mmol/ CS_2CO_3	8	20
4 ^a	TEMPO 0.075 mmol/ CS_2CO_3	8	—
5	TEMPO 0.075 mmol/ $Cu(OAc)_2$ 3 mol%/ CS_2CO_3	8	33

^a In the absence of O_2 .

alcohols as substrates (Table 9). The results revealed that $L_2^{NIS}Cu^{II}/TEMPO$ has good efficiency only for benzyl alcohol and some of its derivatives and not for aliphatic and secondary alcohols. In continuation, we did a comparison between the activity of $L_2^{NIS}Cu^{II}$ and other catalysts that had been proposed in the literature (Table 10).

No reaction was observed in the absence of an additional base, suggesting that the deprotonation of alcohol to alcoholate is necessary prior to the coordination of the substrate to the $Cu(II)$ center. CS_2CO_3 in toluene shows better activity. Cesium cations, with high polarizability and size compared to other alkaline metals, may mainly influence the solubility of CS_2CO_3 in toluene and interaction of CS_2CO_3 with alcohols and consequently, better deprotonation.

There are three different mechanisms for $Cu^{II}/TEMPO$ mediated alcohol oxidation. Stahl's group has shown that the hydrogen transfer to the nitroxyl ligand is the lowest-energy pathway, corresponding to the observed higher conversion percentage of primary alcohols compared to the secondary ones (Scheme 7).³⁴

A proposed mechanism for alcohol oxidation using $L_2^{NIS}Cu^{II}$ is shown in Scheme 8. After coordination of alcoholate to $Cu(II)$, TEMPO as a co-catalyst performs the α H-abstraction from the coordinated alcohol and formation of a ketyl radical in a similar manner to the role of tyrosinate in the enzyme cycle (Scheme 1, B).

It is suggested that an electron transfer to copper produces aldehyde and $Cu(I)$ species and electron and proton transfers from the $Cu(I)$ complex and $TEMPO-H$ return the system back to the original $Cu(II)$ complex and TEMPO. A blank test in the absence of O_2 , benzaldehyde was not produced which proves the role of oxygen in the mechanism (Table 8, entry 4), although the production of H_2O_2 cannot be proven due to difficulty of hydrogen peroxide detection. It is worth mentioning that the coordinated non-innocent ligands facilitate this Cu^{II}/Cu^I ping-pong mechanism.

Table 7 The effect of tempo in the aerobic oxidation of benzyl alcohol by $L_2^{NIS}Cu^{II}$

Entry	Base	Solvent	Catalyst (mol%)	Time (h)	Conversion (%)	
1	TEMPO 5.0×10^{-3}	2 eq. CS_2CO_3	Toluene	2	8	50
2	TEMPO 0.05 mmol	2 eq. CS_2CO_3	Toluene	2	8	80
3	TEMPO 0.05 mmol	2 eq. CS_2CO_3	Toluene	4	8	83
4	TEMPO 0.05 mmol	2 eq. KOH	Toluene	4	8	66
5	TEMPO 0.075 mmol	2 eq. CS_2CO_3	Toluene	3	8	94
6	TEMPO 0.075 mmol	—	Toluene	3	8	25

Table 9 Alcohol oxidation in toluene, catalyzed by $L_2^{NIS}Cu^{II}$ and TEMPO in the presence of Cs_2CO_3 as base and O_2 as oxidant

1. Toluene (2 ml)
2. $L_2^{NIS}Cu^{II}$ (3 mol%)
3. Cs_2CO_3 (2 mmol, 0.65 g)
4. RT, Oxygen
5. TEMPO (0.075 mmol)

Substrate	Product	<i>t</i> (h)	Conversion (%)	Substrate	Product	<i>t</i> (h)	Conversion (%)
		8	94			8	90
		6	94			10	80
		8	90			10	80
		6	94			10	21
		8	90			10	9
		8	93			10	20
		8	95			12	2

B. Homo coupling of alkynes. Alkynes are one of the most important building blocks in organic synthesis, industry and many natural compounds. Hence, scientists have paid much attention to the homo-coupling reaction of terminal alkynes. The mentioned reaction catalyzed by copper complexes represents an effective strategy for the synthesis of the functionalized alkynes. Salkind and Fundyler³⁵ have proposed a mechanism for the mentioned reaction, in which, Cu(I) ions will be coordinated to the alkyne triple bond in a side-on mode and help in C–H activation of this functional group in producing a Cu(II) acetylide complex, which traps the second alkyne. Coupling of these two coordinated alkyne molecules generates the 1,3-diyne as a final product (Scheme 9). The oxidized copper species could be recovered and regenerated by the oxidation with the oxidant to complete the catalytic cycle.

In another part of this work, the Cu(II)-catalyzed homo coupling reaction of terminal alkynes under aerobic conditions was performed. The reaction was done under different reaction conditions (THF, acetonitrile, and toluene as solvents, KOH, Cs_2CO_3 , and Na_2CO_3 as bases and time) (Table 11). The best

achieved conditions are shown in Table 10, entry 7. Homo-coupling of various terminal alkynes that afforded the corresponding symmetrical dienes in excellent yields was then examined under the optimized conditions and summarized in Table 12. Also, the comparison between the activity of $L_2^{NIS}Cu^{II}$ and some other catalysts for phenylacetylene homo-coupling reactions has been given in Table 13. Despite other reports, we have not used unsafe pyridine or other amines such as the expensive base of DABCO *etc.* as additives and harsh conditions.

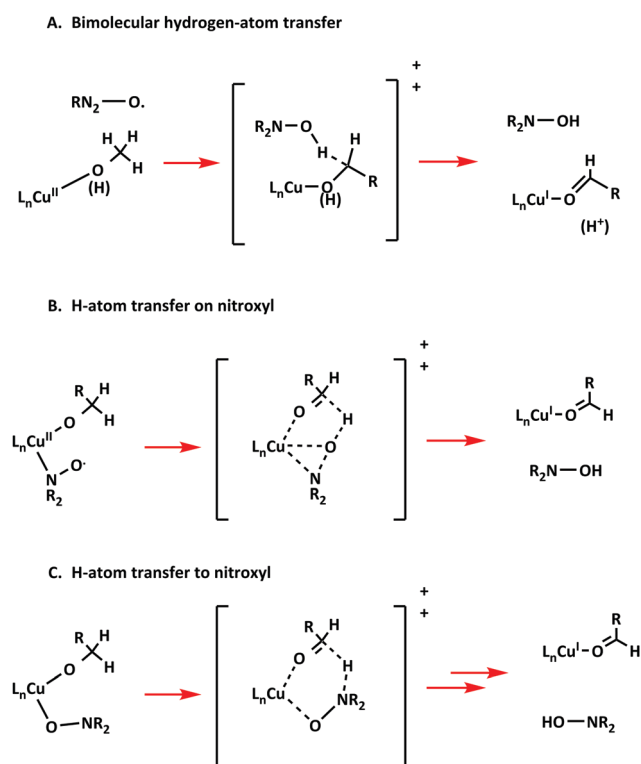
The suggested mechanism is shown in Scheme 10. The coupling process is not effective in the absence of an additional base (Table 11, entry 8). We conclude that the role of the base is deprotonation of acetylene to acetylide and its coordination to the Cu(II) center. This means that the reaction does not proceed through the oxidative addition of acetylide to the Cu(II) center.

Higher conversion values obtained in THF compared to the other solvents seem to be due to the better solubility of the complex in this solvent. In this solvent, KOH showed better activity than NaOH due to the higher basicity of the former.

Table 10 Comparison between the activities of $L_2^{NIS}Cu^{II}$ with other catalysts in alcohol oxidation reaction

	Catalyst (mol%)	Solvent/T (°C)	Time (h)	Yield (%)	Additive	Ref. year
1	$[Cu(CH_3CN)_4]PF_6$ (4)	CH_2Cl_2/RT	3	92	DMAP DBED (0.1 mmol)	27, 2014
2	$Cu^{II}Br_2$ (5)	$MeCN:H_2O/RT$	12	7	KO^tBu (10 mol%) TEMPO (10 mol%)	28, 1977
3	$Cu(ClO_4)_2$ (4)	DMSO/RT	3	100	bpy TMDP TEMPO (6 mol%) DABCO (10 mol%)	29, 2006
4	$L^{APIP}Cu^{II}$ (4)	MeCN/RT	5	100	KOH	7b, 2014
5	$L^{BIS}Cu^{II}OAc$ (4)	Toluene/RT	4	100	CS_2CO_3 , 2 eq.	7a, 2013
6	$[Cu(MeCN)_4](OTf)$ (5)	CH_3CN/RT	20	97	bpy TEMPO (5 mol %)	30, 2010
7	$[(Cu(OOC(C_6H_5)Br)(C_{10}H_9N_3)](ClO_4)$	Water/70	6	71	H_2O_2	31, 2018
8	$CuBr_2$	Acetonitrile:water/RT	2	91	Tetradentate N-donor ligand TEMPO (5 mol%) $t-BuOK$ (5 mol%)	32, 2012
9	Bis[2-(<i>p</i> -tolyliminomethyl)] Phenolato Cu(II) (4)	$CH_3OH/60^\circ C$	1	90	H_2O_2	33, 2015
10	CuL_2^{NIS} (3)	Toluene/RT	8	95	TEMPO (0.075 mmol) CS_2CO_3 (2 eq.)	This work

DMAP = *N,N* dimethylaminopyridine. TEMPO = (2,2,6,6-tetramethylpiperidin-1-yl)oxidanyl. DABCO = 1,4-diazabicyclo[2.2.2]octane.



Scheme 7 Stahl's proposals for mechanism of Cu^{II} /nitroxyl mediated alcohol oxidation.

The reaction was performed under an Ar atmosphere to investigate the importance of oxygen in this coupling process.

As seen in the proposed mechanism (Scheme 10), in the first step, an acetylide ion will be coordinated to the Cu^{II} centre. In the next step, the addition of another acetylide ion and reductive elimination process produce the final product concomitant with

changing the oxidation state of two *o*-iminobenzosemiquinone ligands to *o*-aminophenol.

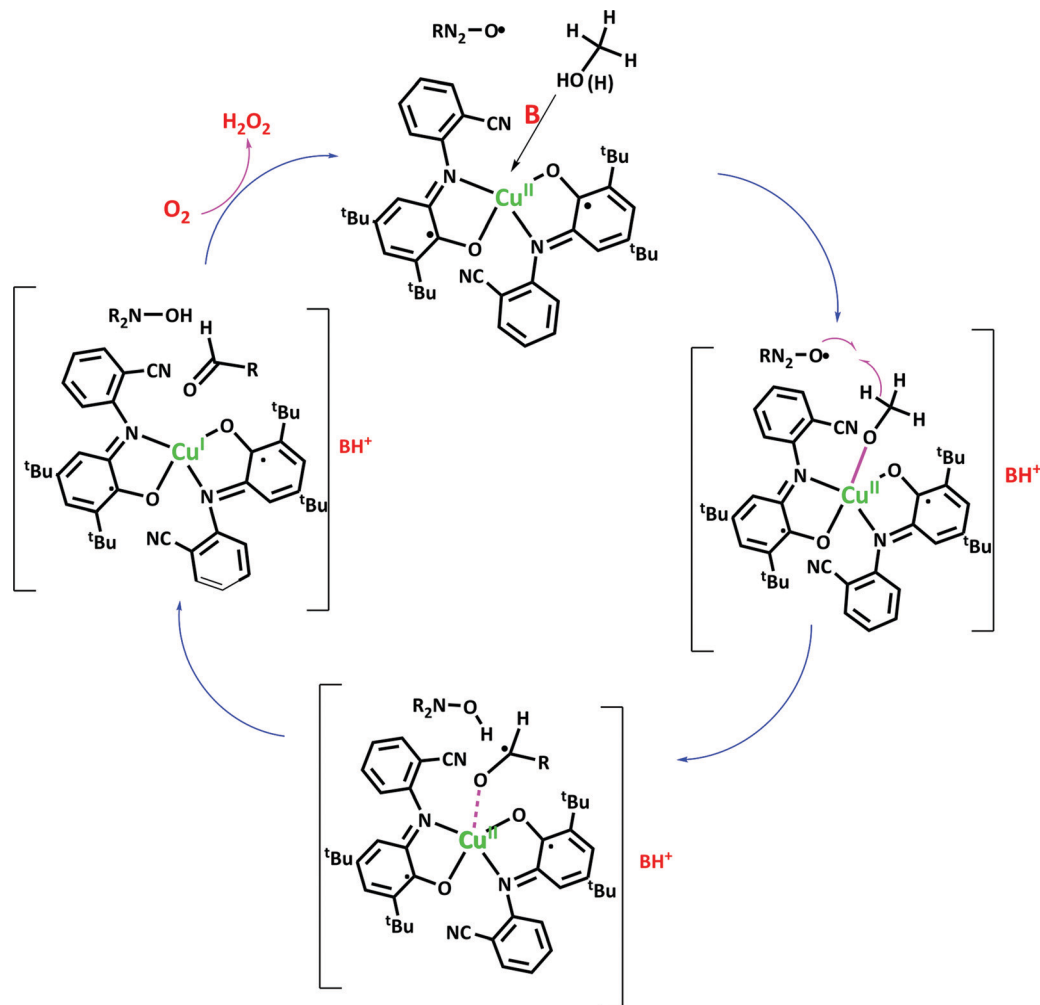
We think that by the reduction of Cu^{II} to $Cu(0)$, both ligands will be disconnected. Therefore, the tuning of oxidation state will be concentrated on the ligands instead of the central metal. Hence, as against other catalysts mentioned in Table 13, we have not used any additive in this reaction. The transformation of O_2 to H_2O_2 in the last copper complex produces the first catalyst. We do not have any proof of our claim about production of H_2O_2 due to difficulty of hydrogen peroxide detection.

The stability of the complex under the reaction conditions was investigated by recording the UV-vis spectrum of $L_2^{NIS}Cu^{II}$ solution in THF before the coupling reaction (without KOH and phenylacetylene addition) and after the reaction (with KOH and phenylacetylene addition) (Fig. S5, ESI†). It is considered that the total feature of the complex spectrum has not considerably changed and we can see a slight shift in the UV and visible parts concomitant with a hyperchromicity in the first and hypochromicity in the latter, which means that the complex structure shows nearly good stability in the presence of KOH.

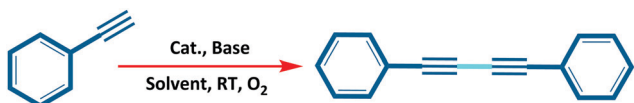
Experimental

Materials and methods

All chemicals and solvents were purchased from Merck, Sigma-Aldrich, Acros, and Fluka and used as received. Electronic spectra were recorded on a Cary 5000 spectrophotometer. IR spectra were recorded in the solid state on an FT-IR Bruker Vector spectrophotometer. Cyclic voltammetry (CV) was performed on a PAR-263A potentiometer, equipped with a Ag wire reference electrode, a glassy carbon working electrode, and a Pt counter electrode with 0.1 M NBu_4ClO_4 solution in CH_2Cl_2 using liquid nitrogen for decreasing the temperature. Ferrocene was used as an



Scheme 8 Possible mechanistic scheme for L₂^{NiS}Cu^{II}/nitroxyl mediated alcohol oxidation.



Scheme 9 Catalytic activity of L₂^{NiS}Cu^{II} in homo-coupling of phenylacetylene.

Table 11 Optimization studies for the L₂^{NiS}Cu^{II}-catalyzed homo coupling reaction of phenylacetylene

Entry	Base	Solvent	Catalyst (mol%)	t (h)	Conversion (%)
1	KOH	THF	1	5	80
2	KOH	THF	2	5	100
3	Cs ₂ CO ₃	THF	2	4.5	100
4	Na ₂ CO ₃	THF	2	6	70
5	KOH	Toluene	2	6	50
6	KOH	Acetonitrile	2	6	50
7	KOH	THF	3	2.5	100
8	—	THF	3	2.5	20

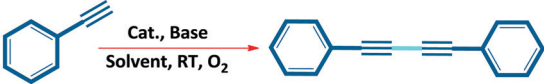
internal standard. The magnetic measurements were obtained with the use of a Quantum Design SQUID magnetometer, MPMS-XL-5. Measurements were performed with 10 mg L^{NiS}Cu^{II} polycrystalline samples. Diamagnetic contribution of the samples was

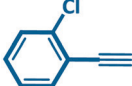
subtracted from the net data sets. EPR spectra were collected using a Bruker EMX plus spectrometer operating with a premium X-band (~9.5 GHz) microwave bridge. Low temperature measurements of a frozen CH₂Cl₂ solution were conducted using a Bruker helium temperature-control system and a continuous flow cryostat. Samples for X-band measurements were placed in 4 mm outer-diameter sample tubes with a volume of ~300 μL. EPR spectra were simulated with the Easy Spin 3.1.7 software.

Synthesis

H₂L^{NAP}. The ligand was synthesized according to the literature.¹⁵ To a mixture of 3,5-di-*tert*-butylcatechol (0.222 g, 1 mmol) and 0.005 mL of triethylamine in *n*-hexane (4 mL), 2-aminobenzonitrile (0.118 g, 1 mmol) was added and the suspension was refluxed for two days and then stirred at room temperature (30 °C) under air for four days. The yellow colour solution turned to red upon stirring. After that, the reaction mixture was kept for crystallization and then re-crystallized thrice from a 1:1 CH₂Cl₂:MeOH solvent mixture for purification. H₂L^{NAP}, a colourless crystalline solid, appeared. Yield: 2.18 g (67.7%). ν_{max}(KBr)/cm⁻¹: 3421 (O-H), 3354 (N-H), and 2222 (–CN) (Fig. S1, ESI[†]).

Table 12 Substrate scope of the Cu-catalyzed C–C homo-coupling between different phenylacetylenes



Substrate	Product	Conversion (%)
		100
		100
		100
		100
		100
		100

Reaction conditions: phenylacetylene derivatives (1 mmol), KOH (2 mmol), $L_2^{NIS}Cu^{II}$ (3 mol%), THF (3 mL), and time (2.5 h).

Table 13 Comparison between the activities of $L_2^{NIS}Cu$ and other catalysts in phenylacetylene C–C homo-coupling reactions

	Catalyst (mol%)	Solvent/ T ($^{\circ}C$)	Time (h)	Yield (%)	Additive	Ref. (year)
1	CuI	H ₂ O/RT	6	99	Et ₃ N (3 eq.)	36 (2014)
	Pd(NH ₃) ₂ (1)				TBAB (0.5 mmol)	
2	CuBr (5)	CH ₃ CN/RT	2	80	Di- <i>tert</i> -butyldiaziridinone (0.9 mmol)	37 (2013)
3	CuI (5)	Acetone/RT	3	91	TMEDA (10 mol%)	38 (2006)
					Et ₃ N (3 mol%)	
4	CuCl ₂ (5)	MeCN/120	1.2	98	TBAF (5 eq.)	39 (2016)
5	CuCl ₂ (3)	Toluene/60	6	99	Et ₃ N (0.03 mmol)	40 (2013)
6	CuI (5)	Solvent-free/RT	12	98	PhCH ₂ NH ₂ (5 mol%)	41 (2014)
7	CuI (4)	30	40 min	86	Pyridine	10 (1960)
8	Cu(OAc) ₂	90	20 min	70	Pyridine	12 (1959)
10 ^a	CuL₂^{NIS} (3)	THF/RT	2.5	100	—	This work

^a KOH (2 eq.). DMAP = *N,N* dimethylaminopyridine. TBAB = tetrabutylammonium bromide. TMEDA = tetramethylethylenediamine. TBAF = tetra-*n*-butylammonium fluoride.

$L_2^{NIS}Cu^{II}$. To a stirred solution of H₂L^{NAP} (0.325 g, 1 mmol) in acetonitrile (10 mL), Cu powder (0.0635 g, 1 mmol) was added. The resulting mixture was stirred for 5 h. Crystals suitable for X-ray diffraction were obtained from a 1:1 CH₂Cl₂:MeOH solvent mixture. Yield: 7.49 g (78%). Anal. calcd (found) for C₄₂H₄₈N₄O₂Cu: C 70.83 (70.93), H 6.75 (6.81), and N 7.86 (7.86). $\nu_{max}(KBr)/cm^{-1}$: 1253 (C–O), 2958, 2940 and 2872 (*tert*-butyl groups), and 2226 (–CN) (Fig. S2, ESI[†]).

Calculations

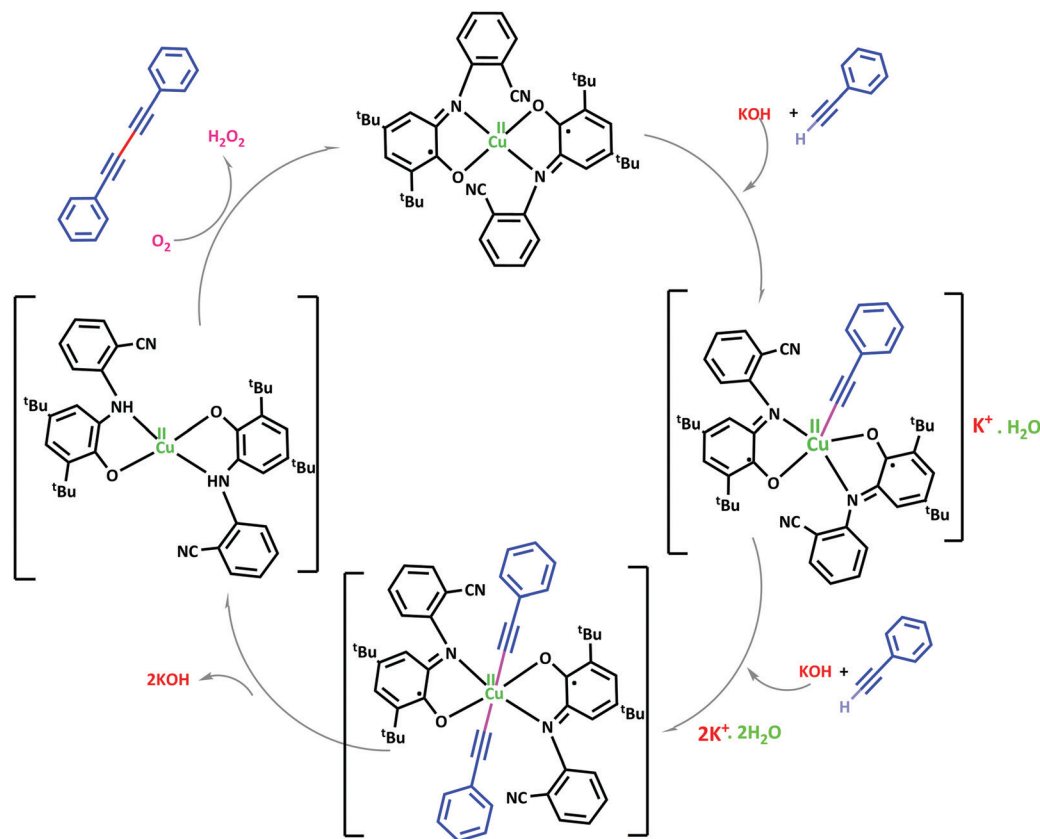
Single point calculations and geometry optimizations were performed using the Gaussian 09 program (Revision E.01),⁴² the B3LYP⁴³/TPSSH⁴⁴ functional, and the 6-311++G(d,p) basis set on all atoms. Broken-symmetry^{45,46} (BS) DFT calculations were performed with the same functional and basis sets. Frequency calculations at the same level of theory confirmed that the optimized structures were located at a minimum on the potential energy surface.

Catalytic activity of the $L_2^{NIS}Cu^{II}$ complex in alcohol oxidation

Alcohol oxidation experiments were carried out in an oxygen atmosphere at room temperature. In a typical experiment, 2 mL of oxygen saturated toluene, alcohol (1 mmol), $L_2^{NIS}Cu^{II}$ (0.017 g, 3 mol%), Cs₂CO₃ (0.650 g, 2 mmol) and TEMPO (0.012 g, 0.075 mmol) was stirred in a 5 mL two-necked flask equipped with an oxygen balloon for the required time. The reaction progress was monitored by gas chromatography. Control reactions were performed using Cu(OAc)₂ and Cs₂CO₃ (0.650 g, 2 mmol) in 2 mL of oxygen saturated toluene under the same conditions described above.

Catalytic activity of the $L_2^{NIS}Cu^{II}$ complex in homo-coupling of phenylacetylene derivatives

In a typical reaction, a mixture of phenylacetylene (1 mmol), KOH (0.112 g, 2 mmol) and $L_2^{NIS}Cu$ (0.017 g, 3 mol%) was stirred in an oxygen atmosphere at room temperature in THF (3 mL).



Scheme 10 Plausible reaction mechanism of homo-coupling of phenylacetylene by $L_2^{NIS}Cu^{II}$.

The reaction progress was monitored by TLC and gas chromatography. After disappearance of phenylacetylene, the product was separated by column chromatography (*n*-hexane/ethyl acetate mixture in 8:1 molar ratio) and characterized by 1H NMR (Fig. S5–S10, ESI †). 1,4-Diphenyl buta-1,3-diyne: 1H NMR (400 MHz, DMSO- d_6) δ 7.69–7.57 (m, 4H), 7.55–7.40 (m, 6H), 1,4-di(pyridin-2-yl)buta-1,3-diyne: 1H NMR (400 MHz, DMSO- d_6) δ 8.66 (ddd, $J = 4.86, 1.76, 0.98$ Hz, 2H), 7.91 (td, $J = 7.75, 1.80$ Hz, 2H), 7.79 (dt, $J = 7.85, 1.13$ Hz, 2H), 7.52 (ddd, $J = 7.65, 4.82, 1.23$ Hz, 2H), 1,4-bis(*p*-fluorophenyl)buta-1,3-diyne: 1H NMR (400 MHz, DMSO- d_6) δ 7.94–7.57 (m, 4H), 7.46–7.02 (m, 4H), 1,4-bis(*p*-tolyl)buta-1,3-diyne: 1H NMR (400 MHz, DMSO d_6) δ 7.50 (d, $J = 7.68$ Hz, 4H), 7.26 (d, $J = 7.75$ Hz, 4H), 2.35 (s, 6H), 1,4-bis(4-methoxyphenyl)buta-1,3-diyne: 1H NMR (400 MHz, DMSO- d_6) δ 7.76–7.40 (m, 4H), 7.04–6.86 (m, 4H), 3.81 (s, 6H), 1,4-bis(2-chlorophenyl)buta-1,3-diyne: 1H NMR (400 MHz, DMSO- d_6) δ 7.79 (dd, $J = 7.67, 1.67$ Hz, 2H), 7.64 (dd, $J = 8.16, 1.19$ Hz, 2H), 7.53 (td, $J = 7.75, 1.67$ Hz, 2H), 7.44 (td, $J = 7.59, 1.26$ Hz, 2H). 47

X-ray analysis

The X-ray data were collected on an Oxford Sapphire CCD diffractometer using MoK α radiation $\lambda = 0.71073$ Å, at 293(2) K, by the ω - 2θ method. The structure has been solved by direct methods and refined with the full-matrix least-squares method on F^2 with the use of the SHELX2014 48 program package. The analytical absorption correction was applied 16,49 (Table 1).

No extinction correction was applied. Hydrogen atoms were located from the electron density maps and their positions were constrained in the refinement. The structural data have been deposited with Cambridge Crystallographic Data Centre, the deposition number being CCDC 1870228. †

Conclusion

In summary, a new Cu(II) complex (CuL^{NIS}) of amino benzonitrile based *o*-aminophenol ligand was synthesized and characterized. In the studied complex, the coordinating ligands were observed in the iminobenzosemiquinone [ISQ^{1-}] radical form. The complex revealed a paramagnetic character caused by the presence of three unpaired electrons located on the *o*-iminobenzosemiquinonate ligands and the Cu(II) center. The complex possesses an $S = 1/2$ ground state which results from strong antiferromagnetic interactions between ligand radicals and weaker ferromagnetic interactions between the copper(II) center and both radicals. The interaction of the redox-active Cu(II) ion and non-innocent L^{NIS} ligands and the properties of non-innocent systems are well developed in this complex. We employed this complex as an efficient catalyst for aerobic oxidation of aromatic alcohols under mild conditions as a model for the galactose oxidase enzyme. Also, the complex was found to be an active catalyst for C–H bond activation and homo-coupling of some terminal alkynes. In both organic transformations, a low amount of the

catalyst in safe media under mild conditions was employed to obtain products in good to excellent yields. Comparison of the alcohol oxidation and C–H activation activity of this catalyst with those of other complexes shows a good to nice activity of this complex. Some other reports of alcohol oxidation protocols, shown in the Results and discussion part, suffer from usage of high amounts of catalyst and TEMPO, and some expensive bases such as DABCO, as well as C–H activation protocols, which are performed under hard conditions, using additives or a high amount of catalyst or bases.

Conflicts of interest

There are no conflicts to declare.

Acknowledgements

The authors are grateful to Shiraz University, and Nicolaus Copernicus University for partial support under Center for Excellence in Research and the BRAIN interdisciplinary research group (AW). E. Safaei is thankful for the financial support of Iran National Science Foundation (INSF)-Grant No. 91002093. Special thanks go to Prof. Andrey Starikov, Prof. John F. Berry, Dr Ekhardt Bill, Dr Zvonko Jagličić, Dr Saeid Zakavi and Dr Touraj Karimpour for their valuable help.

References

- (a) P. J. Chirik and K. Wieghardt, *Science*, 2010, **327**, 794–795; (b) P. L. Holland, *Acc. Chem. Res.*, 2008, **41**, 905–914; (c) B. De Bruin, D. G. Hetterscheid, A. J. Koekkoek and H. Gruetzmacher, *Prog. Inorg. Chem.*, 2007, **55**, 247–354; (d) B. A. Jazdzewski and W. B. Tolman, *Coord. Chem. Rev.*, 2000, **200**, 633–685; (e) P. J. Chirik, *Inorg. Chem.*, 2011, **50**, 9737–9740; (f) M. S. Rogers and D. M. Dooley, *Curr. Opin. Chem. Biol.*, 2003, **7**, 189–196; (g) J. Stubbe and W. A. Van Der Donk, *Chem. Rev.*, 1998, **98**, 705–762; (h) J. W. Whittaker, *Chem. Rev.*, 2003, **103**, 2347–2364.
- B. De Bruin, P. Gualco and N. D. Paul, *Ligand Design in Metal Chemistry: Reactivity and Catalysis*, John Wiley & Sons, 2016, pp. 176–204.
- (a) P. Gamez, I. A. Koval and J. Reedijk, *Dalton Trans.*, 2004, 4079–4088; (b) S. Itoh, S. Takayama, R. Arakawa, A. Furuta, M. Komatsu, A. Ishida, S. Takamuku and S. Fukuzumi, *Inorg. Chem.*, 1997, **36**, 1407–1416; (c) D. J. Kosman, M. J. Ettinger, R. E. Weiner and E. J. Massaro, *Arch. Biochem. Biophys.*, 1974, **165**, 456–467; (d) M. Whittaker and J. W. Whittaker, *J. Biol. Chem.*, 1990, **265**, 9610–9613; (e) N. Ito, S. E. V. Phillips, C. Stevens, Z. B. Ogel, M. J. McPherson, J. N. Keen, K. D. S. Yadav and P. F. Knowles, *Nature*, 1991, **350**, 87–90.
- (a) F. Himo, L. A. Eriksson, F. Maseras and P. E. Siegbahn, *J. Am. Chem. Soc.*, 2000, **122**, 8031–8036; (b) J. W. Whittaker, *Chem. Rev.*, 2003, **103**, 2347–2363.
- N. Ito, S. E. Phillips, K. D. Yadav and P. F. Knowles, *J. Mol. Biol.*, 1994, **238**, 794–814.
- (a) W. Kaim, *Inorg. Chem.*, 2011, **50**, 9752–9765; (b) K. P. Butin, E. K. Beloglazkina and N. V. Zyk, *Russ. Chem. Rev.*, 2005, **74**, 531–553; (c) B. Butschke, K. L. Fillman, T. Bendikov, L. J. Shimon, Y. Diskin-Posner, G. Leitus, S. I. Gorelsky, M. L. Neidig and D. Milstein, *Inorg. Chem.*, 2015, **54**, 4909–4926; (d) C. N. Verani, S. Gallert, E. Bill, T. Weyhermüller, K. Wieghardt and P. Chaudhuri, *Chem. Commun.*, 1999, 1747–1748; (e) S. Itoh, M. Taki and S. Fukuzumi, *Coord. Chem. Rev.*, 2000, **198**, 3–20; (f) Y. Wang, J. L. DuBois, B. Hedman, K. O. Hodgson and T. Stack, *Science*, 1998, **279**, 537–540; (g) Y. Wang and T. Stack, *J. Am. Chem. Soc.*, 1996, **118**, 13097–13098; (h) P. Chaudhuri, M. Hess, U. Flörke and K. Wieghardt, *Angew. Chem.*, 1998, **110**, 2340–2343; (i) P. Chaudhuri, M. Hess, J. Müller, K. Hildenbrand, E. Bill, T. Weyhermüller and K. Wieghardt, *J. Am. Chem. Soc.*, 1999, **121**, 9599–9610; (j) Gabriel M. Duarte, Jason D. Braun, Patrick K. Giesbrecht and David E. Herbert, *Dalton Trans.*, 2017, **46**, 16439–16445; (k) V. Lyaskovskyy and B. de Bruin, *ACS Catal.*, 2012, **2**, 270–279; (l) P. Sarkar and C. Mukherjee, *Dalton Trans.*, 2018, **47**, 13337–13341; (m) G. C. Paul, K. Das, S. Maity, S. Begum and H. K. Srivastava, *Inorg. Chem.*, 2019, **58**, 1782–1793.
- (a) S. Kokatam, *The Coordination Chemistry of Redox Non-innocent O-aminophenol and Dithiolene Ligands with Transition Metal Ions*, 2006; (b) S. E. Balaghi, E. Safaei, L. Chiang, E. W. Wong, D. Savard, R. M. Clarke and T. Storr, *Dalton Trans.*, 2013, **42**, 6829–6839; (c) Z. Alaji, E. Safaei, L. Chiang, R. M. Clarke, C. Mu and T. Storr, *Eur. J. Inorg. Chem.*, 2014, 6066–6074; (d) S. Ghorai and C. Mukherjee, *Chem. – Asian J.*, 2014, **9**, 3518–3524; (e) A. Rajput, A. Saha, S. K. Barman, F. Lloret and R. Mukherjee, *Dalton Trans.*, 2019, **48**, 1795–1813; (f) R. Rakshit and C. Mukherjee, *Eur. J. Inorg. Chem.*, 2016, 2731–2737; (g) R. Rakshit, S. Ghorai, S. Biswas and C. Mukherjee, *Inorg. Chem.*, 2014, **53**, 3333–3337; (h) A. V. Piskunov, I. V. Ershova, M. V. Gulenova, K. I. Pashanova, A. S. Bogomyakov, I. V. Smolyaninov, G. K. Fukin and V. K. Cherkasov, *Russ. Chem. Bull.*, 2015, **64**, 642–649; (i) G. C. Paul, K. Das, S. Maity, S. Begum, H. K. Srivastava and C. Mukherjee, *Inorg. Chem.*, 2018, **58**, 1782–1793; (j) M. K. Mondal and C. Mukherjee, *Dalton Trans.*, 2016, **45**, 13532–13540; (k) A. V. Piskunov, K. I. Pashanova, A. S. Bogomyakov, I. V. Smolyaninov, N. T. Berberova and G. K. Fukin, *Polyhedron*, 2016, **119**, 286–292; (l) M. Bubrin, A. Paretzki, R. Hübner, K. Beyer, B. Schwederski, P. Neugebauer, S. Zális and W. Kaim, *Z. Anorg. Allg. Chem.*, 2017, **643**, 1621–1627; (m) E. Safaei, S. E. Balaghi, L. Chiang, R. M. Clarke, M. Webb, E. W. Y. Wong, D. Savard, C. J. Walsby and T. Storr, *Dalton Trans.*, 2019, **48**, 13326–13336.
- C. Glaser, *Chem. Ber.*, 1869, **2**, 422–424.
- C. Glaser, *Liebigs Ann.*, 1870, **154**, 137–171.
- A. S. Hay, *J. Org. Chem.*, 1960, **25**, 1275–1276.
- G. Eglinton and A. R. Galbraith, *Chem. Ind.*, 1956, **28**, 736–737.
- G. Eglinton and A. R. Galbraith, *J. Chem. Soc.*, 1959, 889–896.
- G. Eglinton, *Adv. Org. Chem.*, 1963, **4**, 225–328.
- (a) A. Sagadevan, V. P. Charpe, A. Ragupathi and K. C. Hwang, *J. Am. Chem. Soc.*, 2017, **139**, 2896; (b) N. Orozco,

- G. Kyriakou, S. K. Beaumont, J. Fernandez Sanz, J. P. Holgado, M. J. Taylor, J. P. Espinós, A. M. Márquez, D. J. Watson, A. R. Gonzalez-Elipse and R. M. Lambert, *ACS Catal.*, 2017, **7**, 3113; (c) D. Chakraborty, S. Nandi, D. Mullangi, S. Haldar, C. P. Vinod and R. Vaidhyanathan, *ACS Appl. Mater. Interfaces*, 2019, **11**, 15670; (d) A. Sagadevan, V. P. Charpe and K. C. Hwang, *Catal. Sci. Technol.*, 2016, **6**, 7688–7692.
- 15 S. Ghorai and C. Mukherjee, *Chem. Commun.*, 2012, **48**, 10180–10182.
- 16 S. N. Brown, *Inorg. Chem.*, 2012, **513**, 1251–1260.
- 17 E. Safaei, H. Bahrami, A. Wojtczak, S. Alavi and Z. Jagličić, *Polyhedron*, 2017, **122**, 219–227.
- 18 P. Chaudhuri, C. N. Verani, E. Bill, E. Bothe, T. Weyhermüller and K. Wieghardt, *J. Am. Chem. Soc.*, 2001, **123**, 2213–2223.
- 19 (a) S.-L. Kokatam, P. Chaudhuri, T. Weyhermüller and K. Wieghardt, *Dalton Trans.*, 2007, 373–378; (b) S. Ghorai, PhD thesis, 2014, <http://gyan.iitg.ernet.in/handle/123456789/557>.
- 20 A. Paretzki, R. Hübner, S. Ye, M. Bubrin, S. Kämper and W. Kaim, *J. Mater. Chem. C*, 2015, **3**, 4801–4809.
- 21 N. F. Chilton, R. P. Anderson, L. D. Turner, A. Soncini and K. S. Murray, *J. Comput. Chem.*, 2013, **34**, 1164–1175.
- 22 (a) J. I. van der Vlugt, *Chem. – Eur. J.*, 2019, **25**, 2651–2662; (b) J. Jacquet, K. Cheaib, Y. Ren, H. Vezin, M. Orio, S. Blanchard, L. Fensterbank, E. Murr and M. Desage, *Chem. – Eur. J.*, 2017, **23**, 15030–15034.
- 23 J. Jacquet, S. Blanchard, E. Derat, M. Desage-El Murr and L. Fensterbank, *Chem. Sci.*, 2016, **7**, 2030–2036.
- 24 L. Noodleman, *J. Chem. Phys.*, 1981, **74**, 5737–5743.
- 25 M. Shoji, K. Koizumi, Y. Kitagawa, T. Kawakami, S. Yamanaka, M. Okumura and K. Yamaguchi, *Chem. Phys. Lett.*, 2006, **432**, 343–347.
- 26 K. Rajabimoghadam, Y. Darwish, U. Bashir, D. Pitman, S. Eichelberger, M. A. Siegler, M. Swart and I. Garcia-Bosch, *J. Am. Chem. Soc.*, 2018, **140**, 16625–16634.
- 27 B. Xu, J. P. Lumb and B. A. Arndtsen, *Angew. Chem.*, 2015, **54**, 4208–4211.
- 28 J. M. Hoover, B. L. Ryland and S. S. Stahl, *ACS Catal.*, 2013, **3**, 2599–2605.
- 29 N. Jiang and A. J. Ragauskas, *J. Org. Chem.*, 2006, **71**, 7087–7090.
- 30 J. M. Hoover, J. E. Steves and S. S. Stahl, *Nat. Protoc.*, 2012, **7**, 1161.
- 31 H. Ünver and I. Kani, *J. Chem. Sci.*, 2018, **130**, 33.
- 32 Z. Hu and F. M. Kerton, *Appl. Catal., A*, 2012, **413**, 332–339.
- 33 M. Hatefi Ardakani, S. Saeednia, M. Mohammadi and E. Mandegari-Kohan, *Inorg. Chem. Res.*, 2016, **1**, 123–130.
- 34 (a) J. M. Hoover and S. S. Stahl, *J. Am. Chem. Soc.*, 2011, **133**, 16901–16910; (b) J. E. Steves and S. S. Stahl, *J. Am. Chem. Soc.*, 2013, **135**, 15742–15745; (c) S. S. Stahl, *Angew. Chem., Int. Ed.*, 2004, **43**, 3400–3420.
- 35 J. S. Salkind and F. B. Fundyler, *Ber. Dtsch. Chem. Ges.*, 1936, **69**, 128–132.
- 36 S. N. Chen, W. Y. Wu and F. Y. Tsai, *Green Chem.*, 2009, **11**, 269–274.
- 37 Y. Zhu and Y. Shi, *Org. Biomol. Chem.*, 2013, **11**, 7451–7454.
- 38 S. Zhang, X. Liu and T. Wang, *Adv. Synth. Catal.*, 2011, **353**, 1463–1466.
- 39 P. B. Thakur and R. K. Kadu, *Imp. J. Interdiscip. Res.*, 2016, **2**, 665–672.
- 40 D. Wang, J. Li, N. Li, T. Gao, S. Hou and B. Chen, *Green Chem.*, 2010, **12**, 45–48.
- 41 G. Cheng, H. Zhang and X. Cui, *RSC Adv.*, 2014, **4**, 1849–1852.
- 42 M. J. Frisch, G. W. Trucks, H. B. Schlegel, G. E. Scuseria, M. A. Robb, J. R. Cheeseman, J. A. Montgomery Jr., T. Vreven, K. N. Kudin, J. C. Burant, J. M. Millam, S. S. Iyengar, J. Tomasi, V. Barone, B. Mennucci, M. Cossi, G. Scalmani, N. Rega, G. A. Petersson, H. Nakatsuji, M. Hada, M. Ehara, K. Toyota, R. Fukuda, J. Hasegawa, M. Ishida, T. Nakajima, Y. Honda, O. Kitao, H. Nakai, M. Klene, X. Li, J. E. Knox, H. P. Hratchian, J. B. Cross, V. Bakken, C. Adamo, J. Jaramillo, R. Gomperts, R. E. Stratmann, O. Yazyev, A. J. Austin, R. Cammi, C. Pomelli, J. W. Ochterski, P. Y. Ayala, K. Morokuma, G. A. Voth, P. Salvador, J. J. Dannenberg, V. G. Zakrzewski, S. Dapprich, A. D. Daniels, M. C. Strain, O. Farkas, D. K. Malick, A. D. Rabuck, K. Raghavachari, J. B. Foresman, J. V. Ortiz, Q. Cui, A. G. Baboul, S. Clifford, J. Cioslowski, B. B. Stefanov, G. Liu, A. Liashenko, P. Piskorz, I. Komaromi, R. L. Martin, D. J. Fox, T. Keith, M. A. Al-Laham, C. Y. Peng, A. Nanayakkara, M. Challacombe, P. M. W. Gill, B. Johnson, W. Chen, M. W. Wong, C. Gonzalez and J. A. Pople, *Gaussian09, Inc.*, Wallingford CT, 2009, **121**, pp. 150–166.
- 43 A. D. Becke, *J. Chem. Phys.*, 1993, **98**, 5648–5652.
- 44 P. Stephens, F. Devlin, C. Chabalowski and M. J. Frisch, *J. Phys. Chem.*, 1994, **98**, 11623–11627.
- 45 L. Noodleman and D. A. Case, *Adv. Inorg. Chem.*, 1992, **38**, 423–470.
- 46 L. Noodleman and E. R. Davidson, *Chem. Phys.*, 1986, **109**, 131–143.
- 47 (a) N. Devarajan, M. Karthik and P. Suresh, *Org. Biomol. Chem.*, 2017, **15**, 9191–9199; (b) M. Guo, B. Chen, M. Lv, X. Zhou, Y. Wen and X. Shen, *Molecules*, 2016, **21**, 606; (c) L. Bettanin, G. V. Botteselle, M. Godoi and A. L. Braga, *Green Chem. Lett. Rev.*, 2014, **7**, 105–112; (d) J. H. Li, Y. Liang and Y. X. Xie, *J. Org. Chem.*, 2005, **70**, 4393–4396; (e) S. N. Chen, W. Y. Wu and F. Y. Tsai, *Green Chem.*, 2009, **11**, 269–274.
- 48 (a) G. Sheldrick, *Acta Crystallogr., Sect. A: Found. Crystallogr.*, 2006, **64**, 112–122; (b) G. Sheldrick, *Acta Crystallogr., Sect. C: Struct. Chem.*, 2015, **71**, 3–8.
- 49 CrysalisPro 1.171.38.43 software, Rigaku OD, 2015.